Ion-Selective Membrane-Coated Graphene−Hexagonal Boron Nitride Heterostructures for Field-Effect Ion Sensing

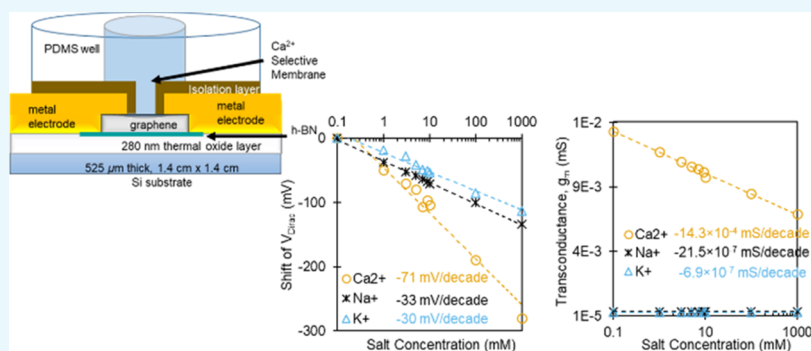Nowzesh Hasan, Urna Kansakar, Eric Sherer, Mark A. DeCoster, and Adarsh D. Radadia*

ACCESS | Metrics & More | Article Recommendations | Supporting Information

ABSTRACT: An intrinsic ion sensitivity exceeding the Nernst−Boltzmann limit and an sp^2-hybridized carbon structure make graphene a promising channel material for realizing ion-sensitive field-effect transistors with a stable solid−liquid interface under biased conditions in buffered salt solutions. Here, we examine the performance of graphene field-effect transistors coated with ion-selective membranes as a tool to selectively detect changes in concentrations of Ca^{2+}, K^+, and Na^+ in individual salt solutions as well as in buffered Locke's solution. Both the shift in the Dirac point and transconductance could be measured as a function of ion concentration with repeatability exceeding 99.5% and reproducibility exceeding 98% over 60 days. However, an enhancement of selectivity, by about an order magnitude or more, was observed using transconductance as the indicator when compared to Dirac voltage, which is the only factor reported to date. Fabricating a hexagonal boron nitride multilayer between graphene and oxide further increased the ion sensitivity and selectivity of transconductance. These findings incite investigating ion sensitivity of transconductance in alternative architectures as well as urge the exploration of graphene transistor arrays for biomedical applications.

1. INTRODUCTION

Ion-sensitive field-effect transistors (ISFETs) have revolutionized the field of ion sensing by reducing the sensor size and response times, enabling mass production, and tighter integration with electronics for drift compensation and data processing.[1−3] Ion sensors play an integral role in biomedical diagnostics,[4] environmental monitoring of water resources,[5,6] and quality control of food and water products.[7] The need for ISFETs with outstanding sensitivity, selectivity, repeatability, response time, and stability in biological fluids remains unaddressed to electronically interface with cells and tissues during the in vitro and in vivo experiments essential to understand the disordered physiological processes associated with diseases or injury and its rapid diagnosis on the bedside.[8] Work to date has explored tailoring the semiconductor−oxide−electrolyte interface using proteins and nucleic acid sequences to selectively detect a wide range of biomolecules,[9,10] increasing the intrinsic sensitivity using various gate dielectric,[11−13] nanoscale channel materials such as silicon nanowires,[14,15] carbon nanotubes,[16,17] organic semiconductors,[18−20] and graphene[21,22] and in situ amplification of the

intrinsic sensitivity using strategies involving dual (solution/bottom) gating[23] and parallel channels of different areas.[24] Graphene and organic semiconductor ISFETs allow overcoming two limiting aspects of silicon analogues. (a) The intrinsic sensitivity for silicon ISFETs due to the oxide−liquid interface has been restricted to the Nernst−Boltzmann limit ($2.3\,k_BT/q$ ~59 mV/decade for monovalent ions) set by the classic Boltzmann distribution of ions at the semiconductor−liquid interface and the site-binding mechanism proposed by Bergveld and co-workers.[25,26] Although intrinsic sensitivity beyond the Nernst−Boltzmann limit has been achieved with silicon ISFETs by reducing ion-binding sites,[27] or controlling the counter-ion size,[28] this requires scaling the transistor channel down to ~25 nm (costly complex lithography) and
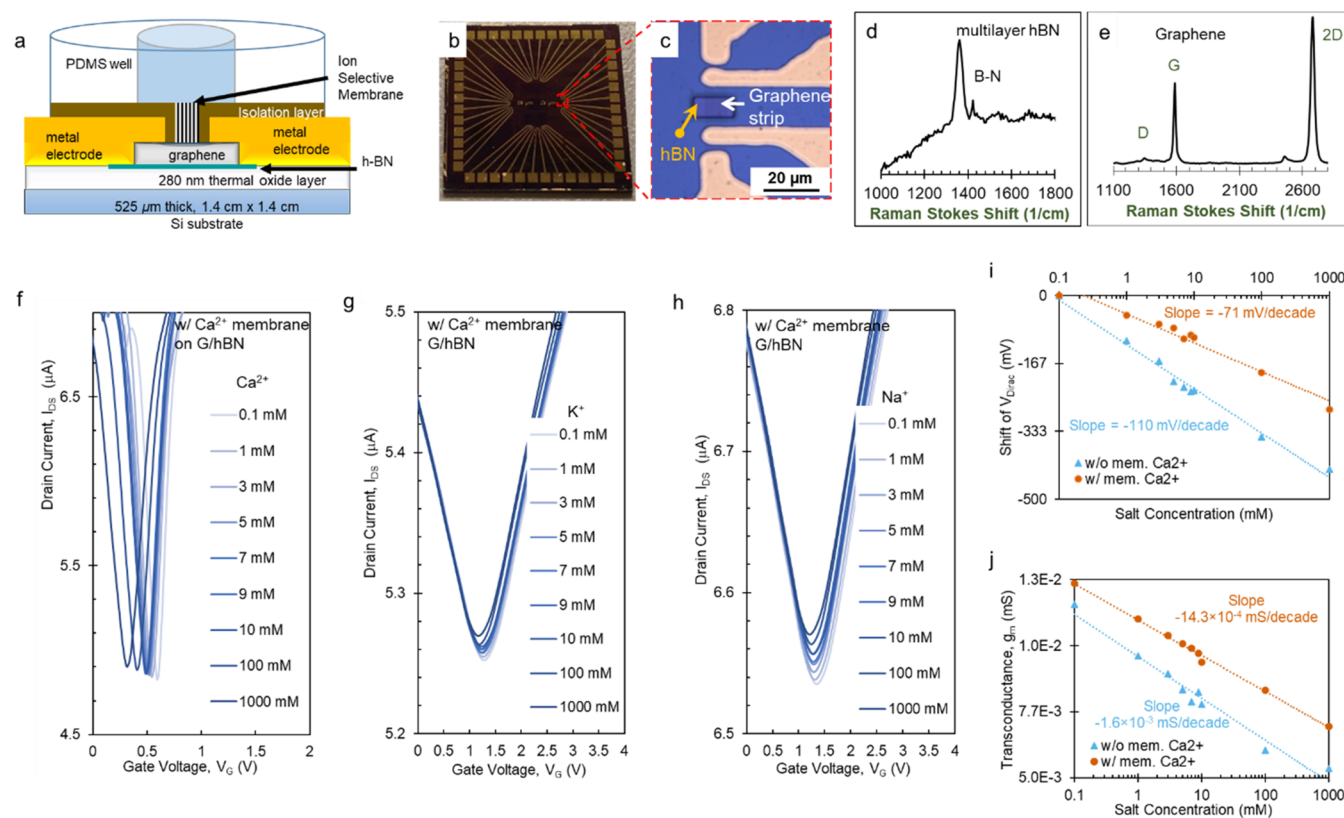
Figure 1. Selective ion sensing demonstrated with calcium ionophore II on an hBN device. (a) Schematic cross-section of the hBN device. (b) Optical image of a chip (1.4 cm × 1.4 cm) that was fabricated for this research, each containing 12 sensors. (c) Optical microscope image of the 70 μm × 10 μm graphene strip spanning across four metal electrodes, all covered with an electrically insulating layer made of SU-8 epoxy. (d) Raman spectrum of multilayer hBN. (e) Raman spectrum of graphene. (f−h) Transfer curves recorded as the membrane-coated graphene on hBN were gated through solutions of (f) CaCl$_2$, (g) KCl, and (h) NaCl of varying concentrations (0.1−1000 mM), in each case. The drain-to-source voltage (V_{DS}) was held constant at 0.1 V. The color intensity of each transfer curve is plot darker for increasing salt concentration. (i) Shift in V_{Dirac} recorded on changing CaCl$_2$ concentration on an hBN device before (blue filled triangles) and after (orange filled circles) casting the Ca^{2+} ion-selective membrane. Shift recorded relative to value at 0.1 mM. (j) Corresponding shift in g_m recorded on the p-carrier dominant side of transfer curves. The dashed lines indicate curves ($y = m \times \log_{10}[x] + c$) fit to the data points of respective color, and the text in the respective color indicates its slope (m).

significant sample preparation. (b) The oxide−liquid interface is sensitive to ion migration especially when solution-gated (the most sensitive way to operate) for prolonged periods in biological electrolytes.[29] The resulting drift in silicon ISFETs is currently addressed in commercial devices (Honeywell DuraFET) through the use of an internal reference, which increases device dimensions.[30] Floating gate design commercialized by Ion Torrent for DNA sequencing also lowers the drift but at the cost of sensitivity.[31]

Intrinsic sensitivity exceeding the Nernst−Boltzmann limit has been demonstrated by our group as well as others with solution-gated ISFETs based on graphene, which due to its sp^2-hybridized carbon network is also expected to be chemically stable when solution-gated in biological electrolytes.[32−34] In prior work, we have shown a sensitivity as high as −164 mV/log[K$^+$] and −57 mV/log[Ca^{2+}] with graphene ISFETs.[33] While the exact transduction mechanism remains unproven, a change in the double-layer composition (both at gate and channel) is believed to be primarily responsible for the observed change in charge carrier concentration and mobility in graphene.[33,35] Enhanced sensitivities up to −198 mV/log[K$^+$] and −110 mV/log[Ca^{2+}] can be obtained by placing graphene on a dangling bond-free, chemically inert substrate such as hexagonal boron nitride (hBN), which is believed to increase the flatness of graphene, improve heat spreading in FETs, and open band gap in graphene leading to enhanced charge carrier mobility, reduced carrier inhomogeneity, and improved high-bias performance.[36−44] This translates to an ion sensitivity normalized with respect to the drain-source voltage of 1980 mV/V/decade between 0.1 and 1000 mM KCl, which is larger than that claimed using organic electrochemical transistors in ref 45. However, to make graphene ISFETs ideal for in vitro and in vivo temporal recording applications such as a neural probe,[46] it is important to induce ion selectivity. Ion-selective solvent-polymeric membrane,[47] similar to those in ion-selective electrodes, holds the potential to induce ion selectivity.[48−51] However, its impact on the inherent ion sensitivity of graphene, the resulting selectivity, and stability in biological electrolytes is unknown.

Here, we characterize the sensitivity, selectivity, and stability of graphene ISFETs coated with ion-selective membranes that are specific to either Na$^+$, K$^+$, or Ca^{2+}. Characterization is performed with respect to shift in Dirac voltage (V_{Dirac}) and transconductance (g_m), which is the slope of the linear region on either side of the transfer curve. A shift in V_{Dirac} indicates a change in the Fermi level of the graphene channel, while a change in g_m indicates a change in charge carrier mobility and/

or gate capacitance. Both V_{Dirac} and g_m follow a Nernst-like (logarithmic) response to changes in ion concentrations. The paper is organized as follows. First, we show the proof-of-principle using ion-selective membranes and characterize its impact on the inherent ion sensitivity of graphene on SiO_2 or hBN. Then, we characterize the sensitivity and selectivity of the Na^+, K^+, and Ca^{2+} ISFETs using individual solutions of NaCl, KCl, and $CaCl_2$, followed by testing in buffered Locke's solution with varying concentrations of either NaCl, KCl, or $CaCl_2$. Finally, we present results on repeatability and stability up to 60 days and discuss the implications of these findings and directions of future research work.

2. RESULTS AND DISCUSSION

2.1. Proof-of-Principle and Impact on Inherent Ion Sensitivity.
ISFET devices (shown in Figure 1a−c) were fabricated with chemical vapor deposition (CVD) graphene directly on a 280 nm thick thermal SiO_2 or with a 13 nm thick hBN spacer layer, here onwards referred to as SiO_2 and hBN devices, respectively. The 200 nm Au/25 nm Cr electrodes were used as the source and the drain, and a poly-(dimethylsiloxane) (PDMS) well was used to hold liquid samples over the device. Graphene and hBN films were characterized via confocal Raman microscopy (Figure 1d,e). Raman spectrum of multilayer hBN exhibited the characteristic E_{2g} phonon mode at 1367 cm^{-1}.[52−54] Raman spectrum of graphene showed a G peak for graphene around 1580 cm^{-1} arising from in-plane vibrations of the sp^2-hybridized carbons,[55−57] a D peak around 1350 cm^{-1} arising from the out-of-plane vibration that for the sp^3-hybridized carbons (defects and residues), and a 2D peak at 2690 cm^{-1} indicating the layer breathing vibration of graphene. The ratio of peak intensities, I_{2D}/I_G, could be strongly affected by the p-doped sample and it decreases with the increase of the doping level as reported in a previous study.[55] The ratio of peak intensities, I_{2D}/I_G (>1), implies that the graphene was monolayer thick. A D* band appearing as a shoulder at ~1615 cm^{-1} on the G band, typically referred to result from defect and edge effects, was not seen in the Raman spectra. A 2500-points Raman mapping was performed over a 50 μm × 50 μm area to examine the quality of transferred graphene, as shown in Figure S1. It shows that the G and 2D peak intensities did not show significant spatial variation, and a separate D* peak was absent. The D peak intensity showed spatial variation, and the defect ratio I_D/I_G was found to be 0.25 ± 0.20 with a distribution shown in Figure S1.

A 2 μm thick SU-8 layer was used to electrically isolate the source and drain electrodes, and a 20 μm × 10 μm window in the SU-8 layer was patterned to expose a 10 μm × 10 μm graphene to the salt solutions during testing. The ion-selective membranes for Na^+, K^+, or Ca^{2+} were formed by drop-casting 1 μL of the ionophore cocktail over the sensor; this resulted in a 1.39 μm thick Na^+ selective membrane, a 1.03 μm thick K^+ selective membrane, or a 32.88 μm thick Ca^{2+} selective membrane as shown in Figure S2. The solutions to cast ion-selective membranes were made as per cocktail solutions sold by a vendor. The Ca^{2+} selective membrane ended up being thicker; this may be intended to reduce the permeation of smaller ions Na+ and K+ and provide higher selectivity. The quantum capacitance of graphene, which is a few μF/cm^2, is high compared to a few hundred nF/cm^2 for a 100 nm thick SiO_2. This, in series with the double-layer capacitance (a few μF/cm^2), allows graphene to be directly gated through the

sample solution without an intermediate insulator layer.[58−60] Detection with graphene ISFET involves recording transfer curves, which are a plot of the drain-to-source current (I_{DS}) as a function of the gate voltage (V_G) typically applied to an Ag/AgCl wire dipped in the sample solution. An ambipolar transfer curve such as those shown in Figure 1f−h is obtained with p-carriers being majority on the right side of the curve, n-carriers being majority on the left side, and both sides meeting at the lowest conductive point, V_{Dirac}. The bidirectional I_d−V_g sweeps in graphene ISFET did show hysteresis in transfer curves, which can be attributed to charge trapping. Reduced hysteresis was found in devices with graphene on hBN. However, to compare the performance of multiple devices with and without hBN, the I_d−V_g sweep was primarily made from positive to negative V_g.

The results reported in this study were collected with five ISFETs with graphene on SiO_2 and three ISFETs with graphene on hBN, here onwards referred to as SiO_2 devices and hBN devices. Three SiO_2 devices and one hBN device were coated with a Ca^{2+} selective membrane, one SiO_2 device and one hBN device were coated with a K^+ selective membrane, and one SiO_2 device and one hBN device were coated with a Na^+ selective membrane. Three SiO_2 devices were characterized in the solutions of varying Ca^{2+} concentrations before and after being coated with a Ca^{2+} selective membrane; here onwards, these results are referred to as without (w/o) ion-selective membrane. This way each device was tested in solutions containing the target cation prior to being coated with a target cation-selective membrane.

Figure 1f−h shows that a Ca^{2+} selective membrane imparts ion selectivity to an hBN device; a relatively larger left shift in V_{Dirac} and a drop in g_m with an increase in Ca^{2+} concentration compared to when Na^+ or K^+ concentrations were varied. The left shift of V_{Dirac} can be explained by the rise in surface potential of graphene, which is expected to increase the doped charge carrier concentration in graphene.[33] This, in turn, is expected to decrease the overall mobility of charge carriers in graphene and thus reduce g_m according to the Drude model. The rise in gate capacitance with ion concentration has little effect on g_m. Figure 1i,j shows a comparison of V_{Dirac} and g_m before and after casting a Ca^{2+} selective membrane on the same hBN device. An overall lower magnitude of V_{Dirac} was obtained for a given $CaCl_2$ concentration, and the ion sensitivity of V_{Dirac} was found to decrease by 36%, from −110 to −70 mV/decade. The magnitude of g_m was found to increase, and the ion sensitivity of g_m on the hBN device reduced from −1.6 × 10^{-3} to −1.4 × 10^{-3} mS/decade but stayed within the same order of magnitude. Similarly, casting a Ca^{2+} ion-selective membrane on a SiO_2 device lowered the overall magnitude of V_{Dirac} and lowered the ion sensitivity of V_{Dirac} by 29%, from −57 to −40 mV/decade (Figure S3). The overall magnitude of g_m was found to increase, and the ion sensitivity of g_m reduced from −2.3 × 10^{-4} to −1.8 × 10^{-4} mS/decade. These performance changes can be explained by the ion screening resulting from the membrane, which decreases the total ions reaching graphene and results in relatively lower doping-induced charge carriers in graphene than when without a membrane. According to the Drude model, the reduced charge carrier concentration leads to an increased charge carrier mobility, and thereby a higher magnitude of g_m and its lower sensitivity to changes in ion concentration.

The reduction of graphene's inherent ion sensitivity by casting a Ca^{2+} selective membrane was confirmed on three
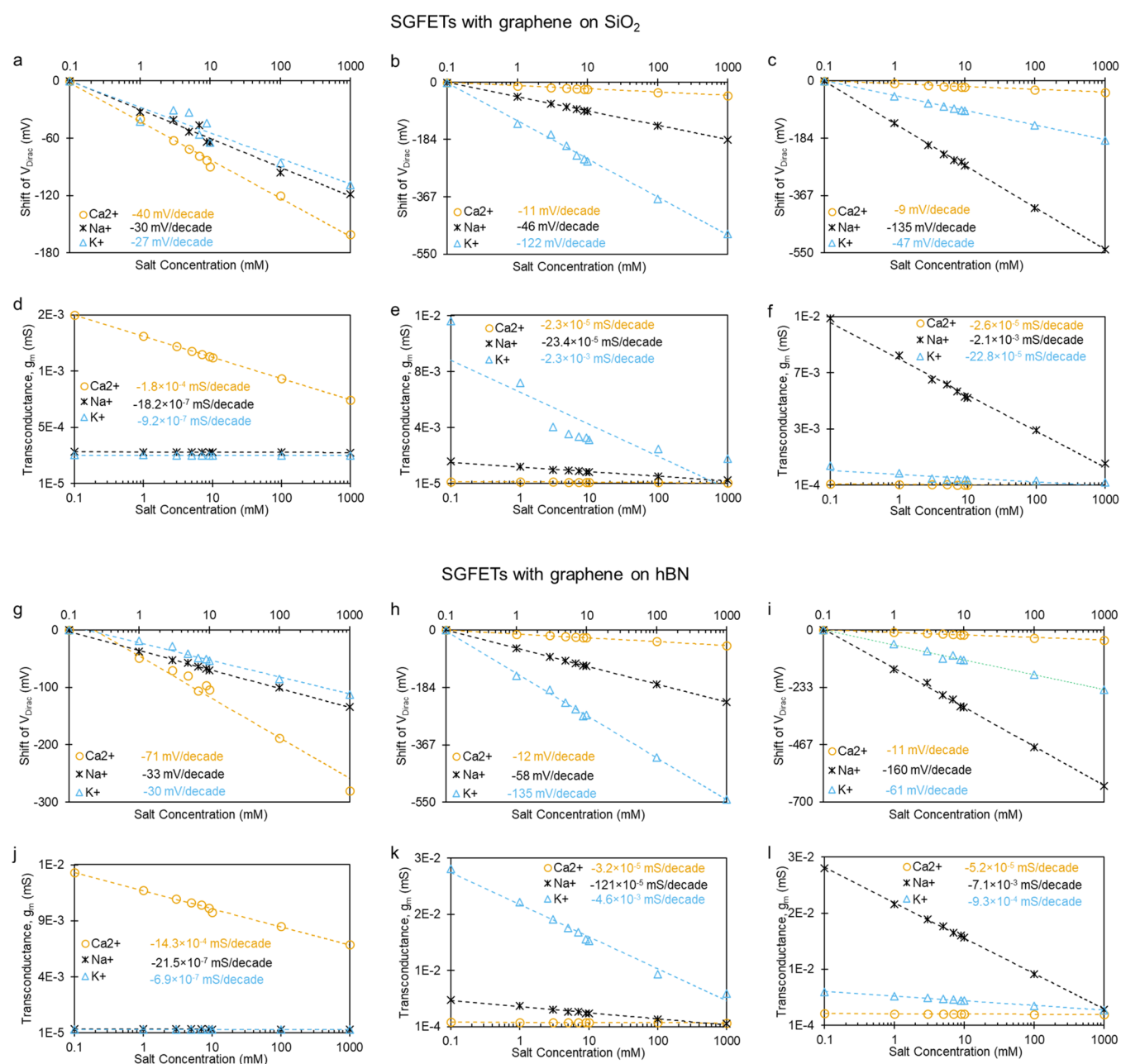
Figure 2. Sensitivity and selectivity evaluated in individual salt solutions. (a−f) Results obtained using SiO_2 devices. (g−l) Results obtained using hBN devices. The left column shows results from devices coated with a Ca^{2+} selective membrane, the middle column shows results from devices coated with a K^+ selective membrane, and the right column shows results from devices coated with a Na^+ selective membrane. (a−c, g−i) The response recorded in terms of the shift in V_{Dirac}. (d−f, j−l) The response recorded in terms of g_m. In each graph, orange circles, black asterisks, and blue triangles represent data recorded in $CaCl_2$, $NaCl$, and KCl, respectively. The dashed lines indicate curves ($y = m \times \log_{10}[x] + c$) fit to the data with respective color, and the text in the respective color indicates its slope.

SiO_2 devices, as shown in Figure S4. Further, the V_{Dirac} and g_m on the hBN device (Figure 1) demonstrated a higher ion sensitivity than SiO_2 devices (Figure S4); the g_m was almost an order magnitude more sensitive to changes in ion concentrations, while the V_{Dirac} was 1.8 times more sensitive. The variation of V_{Dirac} sensitivity among SiO_2 devices was found to range from 2.6 to 12.1%, while the variation of g_m sensitivity was found to range from 9 to 14.5% among SiO_2 devices; this is in agreement to our prior work.[33] Similar experiments were conducted to examine the effect of the K^+ selective and Na^+ selective membranes on the magnitude and ion sensitivity of the V_{Dirac} and g_m on SiO_2 and hBN devices. The results are

presented in Figures S5 and S6. For the K^+ ionophore membrane, the ion sensitivity of V_{Dirac} dropped by 26 and 32% upon membrane coating for the SiO_2 and hBN devices, respectively. For the Na^+ ionophore membrane, the ion sensitivity of V_{Dirac} dropped by 22 and 24% upon membrane coating for the SiO_2 and hBN devices, respectively. The ion sensitivity of g_m reduced in each case but stayed within the same order of magnitude.

2.2. Testing in Individual Salt Solutions. The shift in V_{Dirac} and g_m for the SiO_2 and hBN devices coated with Ca^{2+}, K^+, or Na^+ selective membranes were recorded using 0.1−1000 mM of either Ca^{2+}, Na^+, or K^+ (Figure 2). The shift in V_{Dirac}

was calculated with respect to the lowest ion concentration measured. The slope of the graph plotting the V_{Dirac} or g_m against $\log_{10}$ (ion concentration) was inferred as sensitivity. The selectivity of the ISFET was calculated by taking a ratio of the sensitivity toward the target ion to that toward the interfering ion. For example, when the ion concentration was measured in terms of shift in V_{Dirac}, the Ca^{2+} ionophore membrane on a SiO_2 device in Figure 2a exhibits a selectivity of 1.33 against Na^+ and 1.48 against K^+, respectively. When the sensitivity was measured in terms of g_m, a higher selectivity of ~200 was obtained against both Na^+ and K^+. This was confirmed on three different SiO_2 devices coated with the Ca^{2+} ionophore coating, as shown in Figure S7. Similarly, the sensitivity values from Figure 2 were used to calculate the selectivity values shown in Table 1.

Table 1. Selectivity of ISFETs Measured in the Individual Salt Solution[a]

graphene support				
		No Membrane		
	$S_{V_{Dirac}}^{Ca^{2+}/Na^+}$	$S_{g_m}^{Ca^{2+}/Na^+}$	$S_{V_{Dirac}}^{Ca^{2+}/K^+}$	$S_{g_m}^{Ca^{2+}/K^+}$
SiO_2	0.33	0.13	0.35	0.21
hBN	0.53	0.23	0.56	0.35
		Ca^{2+} Selective Membrane		
	$S_{V_{Dirac}}^{Ca^{2+}/Na^+}$	$S_{g_m}^{Ca^{2+}/Na^+}$	$S_{V_{Dirac}}^{Ca^{2+}/K^+}$	$S_{g_m}^{Ca^{2+}/K^+}$
SiO_2	1.33	98.9	1.48	196
hBN	2.15	665	2.37	2070
		K^+ Selective Membrane		
	$S_{V_{Dirac}}^{K^+/Ca^{2+}}$	$S_{g_m}^{K^+/Ca^{2+}}$	$S_{V_{Dirac}}^{K^+/Na^+}$	$S_{g_m}^{K^+/Na^+}$
SiO_2	11.1	100	2.65	9.83
hBN	11.3	144	2.33	3.80
		Na^+ Selective Membrane		
	$S_{V_{Dirac}}^{Na^+/Ca^{2+}}$	$S_{g_m}^{Na^+/Ca^{2+}}$	$S_{V_{Dirac}}^{Na^+/K^+}$	$S_{g_m}^{Na^+/K^+}$
SiO_2	15	80.8	2.87	9.21
hBN	14.5	137	2.62	7.66

[a] $S_{V_{Dirac}}^{Ca^{2+}/Na^+}$ denotes selectivity of detecting Ca^{2+} over Na^+ with sensitivity measured in terms of the shift in V_{Dirac}. Values rounded to first three accurate digits.

The following observations can be made from the data in Figure 2 and Table 1. (1) Ion selectivity of the devices was enhanced using the ionophoretic membranes as shown by the calculated selectivity of detecting Ca^{2+} in Table 1. For example, the selectivity of Ca^{2+} over Na^+ for the SiO_2 device increased from 0.33 without the ion-selective membrane to 1.33 with the ion-selective membrane. (2) In each of the cases shown in Table 1, the selectivity calculated using g_m exhibits a higher value compared to that calculated using the shift in V_{Dirac}. The values for selectivity measured in terms of g_m exhibited a larger spread, ranging from 3.8 to 2070, while the values for selectivity measured in terms of V_{Dirac} ranged from 1.33 to 15. (3) Compared to SiO_2 devices, hBN devices recorded a larger sensitivity of V_{Dirac} or g_m for the target ion as shown in Figure 2; the gain being the highest for the Ca^{2+} selective membrane and the least for the K^+ selective membrane. In some cases, hBN devices also recorded a larger sensitivity of V_{Dirac} or g_m for the interfering ion. By examining the selectivity values in Table 1, it can be seen that hBN devices yielded an order magnitude higher selectivity for the Ca^{2+} membrane when measured in terms of g_m but a deterioration in selectivity against K^+ on the Na^+ membrane and against Na^+ on the K^+ selective membrane.

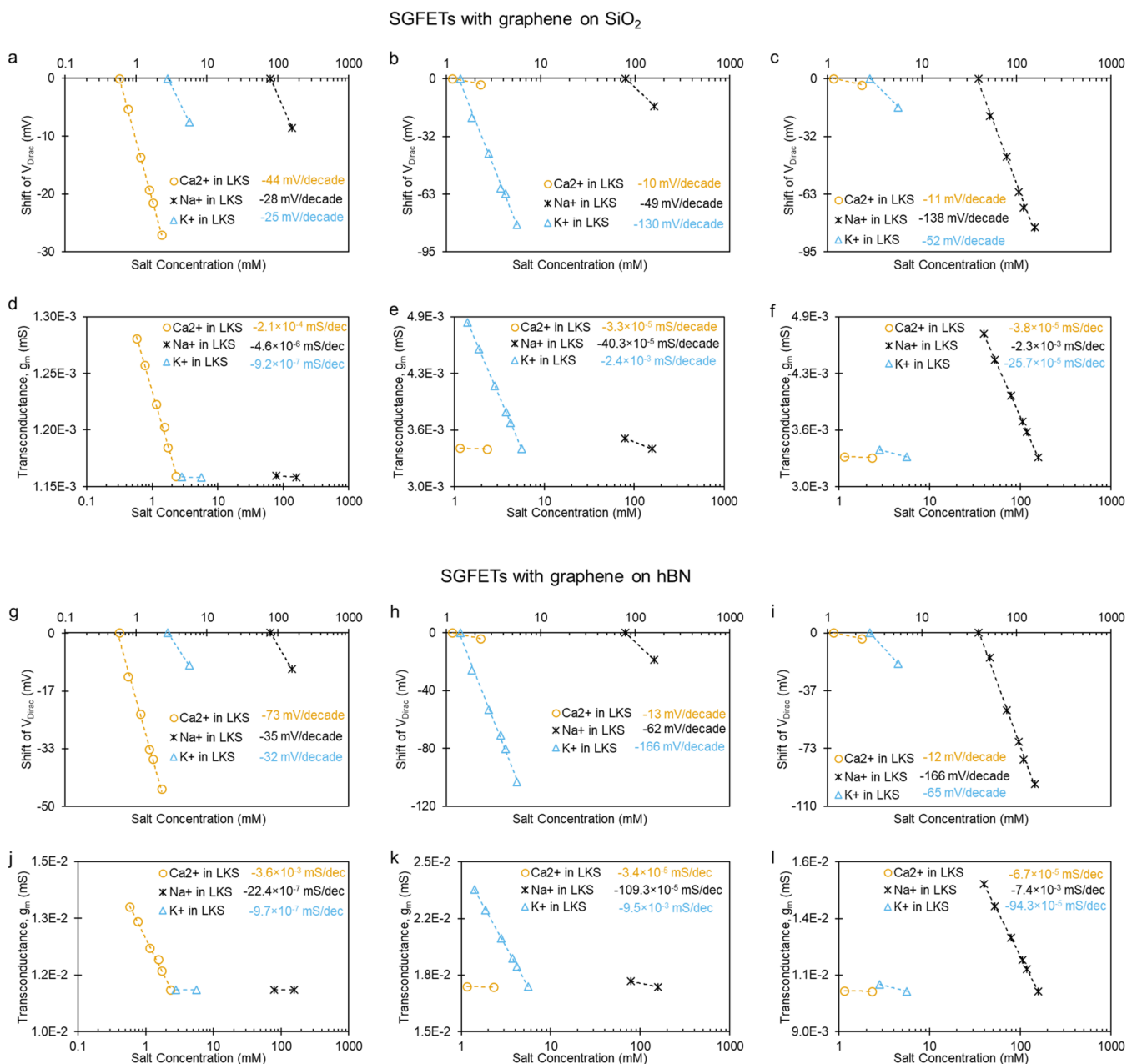**2.3. Testing in HEPES-Buffered Locke's Solution.** The ISFETs were then used to detect changes in concentrations of Ca^{2+}, K^+, and Na^+ in a HEPES-buffered Locke's solution (pH 7.4). The standard Locke's solution formulation used incubate excised brain and for calcium imaging in our lab contains 154 mM NaCl, 5.6 mM KCl, 3.6 mM $NaHCO_3$, 2.3 mM $CaCl_2$, 1.2 mM $MgCl_2$, 5.6 mM glucose, and 5 mM HEPES. Three sets of solutions were prepared by modification of the standard formulation; each set either contained a variation in concentration of Ca^{2+} from 0 to 2.3 mM, K^+ from 0 to 5.6 mM, or Na^+ from 0 to 157.6 mM. The compositions of the nine solutions used in this test are listed in Table S1. The osmolarity was balanced using choline chloride. The changes in V_{Dirac} or g_m of ion-selective membrane-coated ISFETs were recorded in each of these modified Locke's solutions as well as the standard Locke's solution. The results for SiO_2 and hBN devices are shown in Figure 3. The sensitivity values from Figure 3 were used to calculate the selectivity values shown in Table 2.

Comparing the sensitivities measured in terms of shift in V_{Dirac} obtained for the target and interfering ions in Locke's solution (Figure 3) to that obtained in individual salt solutions (Figure 2), it was remarkable that the sensitivities were within 8 mV/decade of each other, except the hBN device coated with K^+ selective membrane, which recorded an increase in sensitivity by 31 mV/decade. Further, the sensitivities measured in terms of g_m using Locke's solution (Figure 3) were found to be within the same order of magnitude with a slight improvement over those recorded in the individual salt solutions (Figure 2); an increase of 2.54 times was recorded in the case of K^+ on the Ca^{2+} selective membrane. Also, it is remarkable that the selectivity values obtained in individual salt solutions (Table 1) are comparable or better than those obtained in Locke's solution (Table 2). The observations (1) and (2) made with testing in individual salt solutions were also noted true when testing with Locke's solution. For each case in Table 2, the selectivity calculated from the shift in g_m exhibits a higher value compared to that calculated using the shift in V_{Dirac}. Also, hBN devices recorded a larger ion sensitivity of V_{Dirac} or g_m for target ions compared to SiO_2 devices, as shown in Figure 3.

Testing sensitivity in Locke's solution also provided an insight into the underlying transduction mechanism of graphene ISFETs. Sensing selectivity in ISFET literature, akin to ion-selective electrodes, has been described using the Nikolsky−Eisenman equation as follows for concentration C of target species i with valency z_i in the presence of other species j with valency z_j.

$$V_{Dirac} \text{ or } g_m = V_0 + A \times \log_{10}\left(C_i + \sum k_j C_j^{z_i/z_j} + L\right) \quad (1)$$

where A is a constant and L is the detection limit. This model assumes that the presence of multiple ionic species induces a competitive binding behavior in the ion-selective membrane and the surface of the ISFET gate at equilibrium. The fitting of data from testing with Locke's solutions (Figure 3) to the Nikolski−Eisenmann equation as per the Bayesian model analysis did not converge as described in the "Bayesian Analysis" section in the Supporting Information. An alternative is to consider the additive binding behavior in the presence of multiple ionic species, which can be explained by the below equation that has been recently described to explain the

Figure 3. Sensitivity and selectivity evaluated in a HEPES-buffered Locke's solution. (a−f) Results obtained using SiO$_2$ devices. (g−i) Results obtained using hBN devices. The left column shows results from devices coated with a Ca^{2+} selective membrane, the middle column shows results from devices coated with a K$^+$ selective membrane, and the right column shows results from devices coated with a Na$^+$ selective membrane. (a−c, g−i) Response recorded in terms of the shift in V_{Dirac}. (d−f, j−l) Response recorded in terms of g_m. In each graph, orange circles, black asterisks, and blue triangles represent data recorded in CaCl$_2$, NaCl, and KCl, respectively. The dashed lines indicate curves ($y = m \times \log_{10}[x] + c$) fit to the data with respective color, and the text in the respective color indicates its slope.

behavior of 0D silicon ISFET with reduced density of charged sites.[27]

$$V_{Dirac} \text{ or } g_m = \text{constant} + \sum_i A_i \log_{10}(C_i) \qquad (2)$$

The data from testing with Locke's solutions (Figure 3) was found to fit eq 2 as shown in the "Bayesian Analysis" section in the Supporting Information. Such additive binding behavior in the ion-selective membrane is highly unlikely due to the vast amount of experimental data showing otherwise. However, such additive binding behavior on the graphene surface potentially would explain why the data fit to eq 2.

2.4. Repeatability and Stability. Repeatability, also called the variability of measurement (instrumental), for a SiO$_2$ device coated with the Ca^{2+} selective membrane was measured by consecutively recording transfer curves thrice while varying CaCl$_2$ concentration in the gating solution from 0.1 to 1000 mM. From these transfer curves, the values for V_{Dirac} and g_m were used to calculate the repeatability, (%)R, as follows

$$(\%)R = \left(1 - \frac{SD}{span}\right) \times 100 \qquad (3)$$

Table 2. Selectivity of ISFETs Measured in a HEPES-Buffered Locke's Solution[a]

graphene support				
	Ca^{2+} Selective Membrane			
	$S_{V_{Dirac}}^{Ca^{2+}/Na^+}$	$S_{g_m}^{Ca^{2+}/Na^+}$	$S_{V_{Dirac}}^{Ca^{2+}/K^+}$	$S_{g_m}^{Ca^{2+}/K^+}$
SiO$_2$	1.57	45.4	1.76	228
hBN	2.09	1610	2.28	3710
	K$^+$ Selective Membrane			
	$S_{V_{Dirac}}^{K^+/Ca^{2+}}$	$S_{g_m}^{K^+/Ca^{2+}}$	$S_{V_{Dirac}}^{K^+/Na^+}$	$S_{g_m}^{K^+/Na^+}$
SiO$_2$	13	72.7	2.65	5.96
hBN	12.8	279	2.67	8.69
	Na$^+$ Selective Membrane			
	$S_{V_{Dirac}}^{Na^+/Ca^{2+}}$	$S_{g_m}^{Na^+/Ca^{2+}}$	$S_{V_{Dirac}}^{Na^+/K^+}$	$S_{g_m}^{Na^+/K^+}$
SiO$_2$	12.6	60.5	2.65	8.95
hBN	13.8	111	2.55	7.85

[a]$S_{V_{Dirac}}^{Ca^{2+}/Na^+}$ denotes selectivity of detecting Ca^{2+} over Na$^+$ with sensitivity measured in terms of the shift in V_{Dirac}. Values rounded to first three accurate digits.

where SD represents the standard deviation among recorded values for V_{Dirac} or g_m and span is the maximum value among three trials. The obtained values for V_{Dirac} and g_m are plotted in Figure S8. The calculated values of standard deviation, span, and $1 - (\%)R$ are tabulated in Table S2. The plot of normalized standard deviation (SD/span) in V_{Dirac} values as a function of CaCl$_2$ concentrations did not show a discernable trend as evident from Figure 4a; an average value of 0.28% and a maximum value of 0.44% were obtained. The average $(\%)R$ in the measurement of V_{Dirac} was calculated to be 99.56%. Likewise, the normalized standard deviation in g_m was also found not to be a discernable function of CaCl$_2$ concentration, as shown in Figure 4b; an average normalized standard deviation of 0.03% and a maximum value of 0.07% were obtained. The average $(\%)R$ in the measurement of g_m was calculated to be 99.93%, which is superior to 99.5% obtained with current commercial ISFETs (Microsens MSFET-3330). The lack of such data for coated commercial ISFETs made it difficult to make a direct comparison.

The stability of a SiO$_2$ device coated with a Ca^{2+} selective membrane was gauged by conducting an experiment at regular intervals (15 days) for a total period of 60 days. In each experiment, a transfer curve was recorded while gating through CaCl$_2$ concentrations ranging from 0.1 to 1000 mM. The V_{Dirac} and g_m values were seen to increase with time as shown in the plot for 10 mM CaCl$_2$ in Figure 4c,d. The data for the rest of

the concentrations is provided in Figures S9 and S10. Reproducibility $(\%)R_p$ was calculated using eq 1 with SD now calculated as the standard deviation in V_{Dirac} or g_m values over the 60 days and span as the maximum value obtained over the 60 days. The detailed calculation of $(\%)R_p$ for V_{Dirac} and g_m is provided in Tables S3 and S4, respectively. The value for $(\%)R_p$ in the measurement of V_{Dirac} ranged between 98.45 and 99.12%. Similarly, the value for $(\%)R_p$ in the measurement of g_m ranged between 98.34 and 98.92%. The average ion sensitivity of V_{Dirac} and g_m over the 60 days was found to be -39.2 ± 0.6 mV/decade and $-2 \times 10^{-4} \pm 3.6 \times 10^{-6}$ mS/decade, respectively, with a maximum deviation of 3.8 and 4.3%, respectively (see Figure S11). A higher value of $(\%)R_p$ translates to less frequent calibrations for continuous monitoring applications. The values of $(\%)R_p$ obtained here are far superior compared to most nonencapsulated silicon-based ISFETs, which have a characteristic drift of ~1 mV/h, which further translates to a $(\%)R_p$ value of 90%. Ruggedized encapsulation of silicon ISFETs such as in the case of Honeywell DuraFET has allowed achieving $((\%)R_p)$ values of 99.5%.

2.5. Practical Implications. Here, we showed that monitoring g_m on hBN devices coated with ion-selective membranes allowed sensing changes in concentrations of Ca^{2+}, K$^+$, and Na$^+$ with good sensitivity, selectivity, repeatability, and stability. For example, with the Ca^{2+} membrane-coated hBN device, the fluctuation of K$^+$ concentration from 5.6 to 2.8 mM and Na$^+$ concentration from 157.6 to 78.8 mM in Locke's solution resulted in a change in g_m equivalent to that would have resulted from the standard Ca^{2+} concentration of 2.3 mM to change by 0.4 and 1 μM, respectively. Similarly, with the K$^+$ membrane-coated hBN device, the fluctuation of Ca^{2+} concentration from 2.3 to 1.15 mM and Na$^+$ concentration from 157.6 to 78.8 mM in Locke's solution resulted in a change in g_m equivalent to that would have resulted from the standard K$^+$ concentration of 5.6 mM to change by 13 μM and 0.46 mM, respectively. Likewise, with the Na$^+$ membrane-coated hBN device, the fluctuation of Ca^{2+} concentration from 2.3 to 1.15 mM and K$^+$ concentration from 5.6 to 2.8 mM in Locke's solution resulted in a change in g_m equivalent to that would have resulted from the standard Na$^+$ concentration of 157.6 mM to change by 1 and 14.5 mM, respectively.

A parallelization could conceivably be achieved for the synchronized detection of Na$^+$, K$^+$, and Ca^{2+} using a sensor array of ISFETs coated alternately with solvent-polymeric membranes specific to Na$^+$, K$^+$, and Ca^{2+}. Such sensing arrays
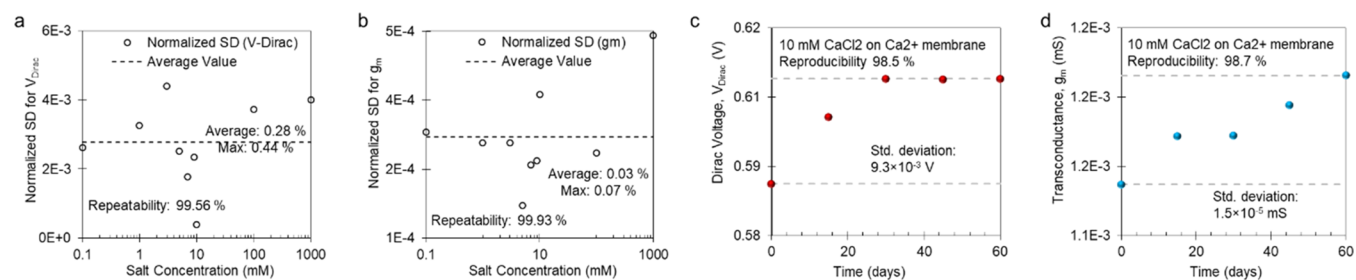
Figure 4. Repeatability and stability measurements for ISFETs coated with the Ca^{2+} selective membrane cast on a SiO$_2$ device. (a, b) Normalized standard deviation in the measurement of V_{Dirac} (a) and (b) g_m as a function of CaCl$_2$ concentration during three separate experiments on the same device. The black hollow circles are data points corresponding to CaCl$_2$ concentration tested, and the dashed black lines show the average value. (c) V_{Dirac} and (d) g_m measured when the same device was gated using fresh 10 mM CaCl$_2$ at different time points. The filled red and blue circles are data points indicating V_{Dirac} and g_m, respectively, and the dashed gray lines indicate the extremes recorded.

would be of immense value on a Petri dish or a neural probe for the detection of extracellular ion concentrations. Body fluid concentrations of the three most important cations, Na^+ (135−145 mM), K^+ (3.5−5.0 mM), and Ca^{2+} (1.1−1.3 mM) are tightly regulated for normal functions. While Na^+ levels maintain an osmotic balance and a control over fluid movement between compartments, the Ca^{2+} and K^+ levels help establish membrane potentials essential for firing or resting in neurons and muscle fibers. Studying the dynamics of these cations concurrently could conceptually help improve our understanding of how abnormal functions result in a complex organ like the brain.[61,62] However, in our experiments, we did not optimize membrane formulations, they were adapted from the literature,[63] and low volumes of it were cast to achieve the thinnest films. To realize highly sophisticated arrays of ISFETs in a Petri dish or a neural probe, the following should be considered. The concentrations of ionophore, plasticizer, and additives as well as the membrane thickness could be optimized to achieve an application-specific balance between sensitivity, selectivity, and response time. In addition, this optimization has to be done at the target operating temperature, which would be 37 °C for most biological experiments. Further, it is difficult to infer the concentration of a specific ion with high confidence using g_m recorded on a single ISFET. This confidence could be improved using duplicate ISFETs, reference ISFETs, and using membranes doped with other target-specific ionophores; however, this would increase the device size or decrease spatial resolution. Alternatively, results from ISFETs for detecting other expected ions, like that reported here, can be correlated to increase the confidence in reporting ion concentration and also identifying a change in the concentration of more than one ion. The results of such a combination of sensors can be bolstered with the use of nonlinear signal processing methods such as the partial least squares regression, artificial neural networks, and Bayesian blind source separation to confidently reconstruct ion concentrations.

3. CONCLUSIONS

In summary, we evaluated different aspects of ISFETs coated with ion-selective membranes to selectively detect changes in concentrations of Ca^{2+}, K^+, and Na^+ in solution. The membrane coating lowers the inherent sensitivity of the V_{Dirac} and g_m in an ISFET but imparts noticeable selectivity toward the target ion. The graphene−hBN heterostructure results in devices with higher ion sensitivity of V_{Dirac} and g_m compared to devices with graphene on SiO_2. Results from testing with individual salt solutions and buffered Locke's solutions show that in comparison to V_{Dirac}, monitoring g_m provides a higher selectivity in sensing targeted ions. Both V_{Dirac} and g_m were measured with greater than 99.5% repeatability. Using experiments over 60 days, we show that measurements of V_{Dirac} and g_m are more than 98% reproducible and the ion sensitivity of V_{Dirac} and g_m stays within 3.8 and 4.3% of that recorded at day 0, respectively. This demonstrates the stability of the membrane−graphene structure in a biological electrolyte. These results warrant the use of graphene ISFET-based tools for biological studies sensing ion concentration changes outside the cell.

4. METHODOLOGY AND MATERIALS

4.1. Materials. Copper foils (20 μm thick) with monolayer graphene or multilayer hBN films grown by the chemical vapor deposition (CVD) method were obtained from Graphene Labs Inc. These CVD graphene films were 1−10 μm in grain size and mostly monolayer with 10−30% bilayer islands. Poly-(methyl methacrylate) (996 kDa) was obtained from ALDRICH, and it was dissolved in anisole from Fluka to prepare a 5 (w/v)% PMMA solution. Copper etchant type CE-100 was obtained from TRANSENE Company, Inc. A general method to transfer hBN and graphene films from copper to silicon substrates as required to build the needed devices is described in ref 33.

4.2. Raman Spectroscopy. Raman spectroscopy was carried using a Horiba Scientific XploRA Plus confocal Raman microscope equipped with a 532 nm laser, 100 × 0.95 NA objective 1200 lines/mm diffraction grating, a 300 μm slit, and a 200 μm hole. The setup achieved a beam spot diameter of 1 μm. Raman spectrum for mono/bilayer CVD graphene and multilayer hBN exhibits characteristic peaks, as shown in Figure 1c,d.

4.3. Ion-Selective Cocktail Preparation and Film Deposition. The ion-selective membrane solution was prepared by dissolving the ion-selective cocktail with the corresponding solvent. The sodium ion-selective membrane cocktail comprised of sodium ionophore X (1% w/w; Selectophore, Sigma-Aldrich), sodium tetrakis [3,5-bis-(trifluoromethyl)phenyl] borate (0.55% w/w; Selectophore, Sigma-Aldrich), poly(vinyl chloride) (33% w/w; Sigma-Aldrich), and bis(2-ethylhexyl) sebacate (65.45% w/w; Sigma-Aldrich). The sodium ion-selective membrane solution was prepared by dissolving 100 mg of the ion-selective cocktail in 660 μL of tetrahydrofuran (anhydrous, ≥99.9%; Sigma-Aldrich).[63,64] The potassium ion-selective membrane cocktail comprised of valinomycin (2% w/w; Sigma-Aldrich), sodium tetraphenyl borate (0.6% w/w; Sigma-Aldrich), poly(vinyl chloride) (32.7% w/w; Sigma-Aldrich), and bis(2-ethylhexyl) sebacate (64.7% w/w; Sigma-Aldrich). The potassium ion-selective membrane solution was prepared by dissolving 100 mg of the ion-selective cocktail in 350 μL of cyclohexanone (≥99.5%; Selectophore, Sigma-Aldrich). The calcium ion-selective membrane cocktail comprised of calcium ionophore II (9.2% w/w; Selectophore, Sigma-Aldrich), sodium tetrakis-[3,5-bis(trifluoromethyl)phenyl]borate (4.5% w/w; Selectophore, Sigma-Aldrich), bis(2-ethylhexyl) sebacate (56.3% w/w; Sigma-Aldrich), and poly(vinyl chloride) (30% w/w; Sigma-Aldrich). The calcium ion-selective membrane solution was prepared by dissolving 111 mg of the ion-selective cocktail in 333 mg of tetrahydrofuran (anhydrous, ≥99.9%; Sigma-Aldrich). The ionophore membrane was coated on the exposed graphene surface by drop-casting 1 μL of the ion-selective solution over a 20 μm × 10 μm sensing window using the solvent evaporation process at room temperature (25 °C).

4.4. Ion-Selective HEPES-Buffered Locke's Solution. Within 248.75 mL of purified deionized water, 2250 mg of NaCl (154 mM), 104.4 mg of KCl (5.6 mM), 75.6 mg of $NaHCO_3$ (3.6 mM), 84.5 mg of $CaCl_2 \cdot 2H_2O$ (2.3 mM), 61 mg of $MgCl_2 \cdot 6H_2O$ (1.2 mM), and 252.3 mg of $C_6H_{12}O_6$ (5.6 mM) were dissolved via vortexing. Then, 1.25 mL of 1 M stock $C_8H_{18}N_2O_4S$ (5 mM) with pH 7.4 was added into the dissolved solution. Within a vacuum chamber, the dissolved liquid was passed through the filter using vacuum filtration.

The HEPES-buffered fluid was stored inside the refrigerator under 4 °C.

4.5. Electrical Measurements. All electrical measurements were accomplished with a probe station inside a Faraday cage. Resistance and transfer curves were measured using a dual source-measurement unit (Keithley 2636A). A poly-(dimethylsiloxane) (PDMS) well was punched out to hold the electrolyte over the graphene strip. Electrochemical top-gate circuit setup was completed by immersing an Ag/AgCl electrode into the electrolyte. The resistance of the graphene strip was measured in air by sweeping the drain-to-source voltage (V_{DS}) from 0 to 100 mV in pulsed mode (1 ms pulse width, 50 ms time period). The pulsed mode was used to avoid significant Joule heating effects during measurements. Over ion-selective membranes (Ca^{2+}, Na^+, and K^+), electrolytes (NaCl, KCl, and $CaCl_2$) of varying concentration (0.1, 1, 3, 5, 7, 9, 10, 100, and 1000 mM) were used as the gate electrolyte in measuring transfer curves on graphene ISFETs with or without hBN as an underlying dielectric layer. To generate transfer curves, V_{DS} was held constant at 100 mV DC across the drain and the source while sweeping the gate voltage, V_G. Using the Ca^{2+} ionophore membrane on graphene ISFET over SiO_2, three trials of transfer curve measurement data are recorded using $CaCl_2$ with varying concentrations (0.1–1000 mM) for testing repeatability. For sensor stability testing, five sets of transfer curve measurement data are recorded with the Ca^{2+} ionophore membrane on graphene ISFET fabricated on SiO_2 over 15 days apart. In both cases for repeatability and reproducibility data recording, V_{DS} was held constant at 100 mV DC across the drain and the source while sweeping the gate voltage. For the Ca^{2+} ionophore membrane, using varying Ca^{2+} concentrations (0, 0.58, 0.77, 1.15, 1.53, 1.73, and 2.3 mM) in Locke's solutions, transfer curves are recorded from graphene ISFETs with and without hBN. To observe the selectivity, transfer curves are recorded with varying Na^+ concentrations (0, 78.8, and 157.6 mM) and K^+ concentrations (0, 2.8, and 5.6 mM) in Locke's solutions. Likewise, for the Na^+ ionophore membrane, using varying Na^+ concentrations (0, 39.4, 52.53, 78.8, 105.07, 118.2, and 157.6 mM) in Locke's solutions, transfer curves are recorded from graphene ISFETs with and without hBN. To observe the selectivity, transfer curves are recorded with varying Ca^{2+} concentrations (0, 1.15, and 2.3 mM) and K^+ concentrations (0, 2.8, and 5.6 mM) in Locke's solutions. For the K^+ ionophore membrane, using varying K^+ concentrations (0, 1.4, 1.87, 2.8, 3.7, 4.2, and 5.6 mM) in Locke's solutions, transfer curves are recorded from graphene ISFETs with and without hBN. To observe the selectivity, transfer curves are recorded with varying Ca^{2+} concentrations (0, 1.15, and 2.3 mM) and Na^+ concentrations (0, 78.8, and 157.6 mM) in Locke's solutions.

ASSOCIATED CONTENT

Ⓢ Supporting Information

The Supporting Information is available free of charge at https://pubs.acs.org/doi/10.1021/acsomega.1c02222.

> Figure S1: Raman mapping of transferred graphene; Figure S2: change in ion-selective membrane film thickness and diameter with varying amount of membrane cocktail solution; Figure S3: selective ion sensing demonstrated with calcium ionophore II on a SiO_2 device; Figure S4: impact of casting the Ca^{2+} selective membrane on the sensitivity of g_m and V_{Dirac}

to changes in $CaCl_2$ concentrations; Figure S5: impact of casting the K^+ selective membrane on the sensitivity of V_{Dirac} and g_m to changes in KCl concentrations; Figure S6: impact of casting the Na^+ selective membrane on the sensitivity of g_m and V_{Dirac} to changes in NaCl concentrations; Figure S7: response of Ca^{2+} selective membrane-coated SiO_2 devices recorded in single-salt solutions (NaCl, KCl, or $CaCl_2$); Figure S8: repeatability measurements for ISFETs coated with the Ca^{2+} selective membrane on the SiO_2 device; Figure S9: reproducibility of V_{Dirac} for a SiO_2 device coated with the Ca^{2+} selective membrane; Figure S10: reproducibility of g_m for a SiO_2 device coated with the Ca^{2+} selective membrane; Figure S11: ion sensitivity of V_{Dirac} and g_m over 60 day period for a SiO_2 device coated with the Ca^{2+} selective membrane; Table S1: repeatability calculation using normalized standard deviations in (a) Dirac voltage (V_{Dirac}) and (b) transconductance (g_m) based on three consecutive trials; Table S2: reproducibility calculation using V_{Dirac} recorded over a period of 60 days when measured with different $CaCl_2$ solutions; Table S3: reproducibility calculation using g_m recorded over a period of 60 days when measured with different $CaCl_2$ solutions (0.1–1000 mM); Table S4: composition of solutions that were used to obtain results in Figure 3; and A section on Bayesian analysis of data in Figure 3 (PDF)

AUTHOR INFORMATION

Corresponding Author

    Adarsh D. Radadia − *Institute for Micromanufacturing, Louisiana Tech University, Ruston, Louisiana 71272, United States; Center for Biomedical Engineering and Rehabilitation Sciences and Chemical Engineering, Louisiana Tech University, Ruston, Louisiana 71272, United States;* ⓘ orcid.org/0000-0002-2791-0421; Email: radadia@latech.edu

Authors

    Nowzesh Hasan − *Institute for Micromanufacturing, Louisiana Tech University, Ruston, Louisiana 71272, United States; Center for Biomedical Engineering and Rehabilitation Sciences, Louisiana Tech University, Ruston, Louisiana 71272, United States;* Present Address: Lawrence Berkeley National Laboratory, Berkeley, California 94720, United States

    Urna Kansakar − *Institute for Micromanufacturing, Louisiana Tech University, Ruston, Louisiana 71272, United States; Center for Biomedical Engineering and Rehabilitation Sciences, Louisiana Tech University, Ruston, Louisiana 71272, United States;* Present Address: Albert Einstein College of Medicine, Bronx, New York 10461, United States.

    Eric Sherer − *Chemical Engineering, Louisiana Tech University, Ruston, Louisiana 71272, United States;* Present Address: Corteva Agriscience, Indianapolis, Indiana 46268, United States.

    Mark A. DeCoster − *Institute for Micromanufacturing, Louisiana Tech University, Ruston, Louisiana 71272, United States; Center for Biomedical Engineering and Rehabilitation Sciences, Louisiana Tech University, Ruston, Louisiana 71272, United States*

Complete contact information is available at:
https://pubs.acs.org/10.1021/acsomega.1c02222

Author Contributions

N.H. and A.D.R. conceived and designed the experiments; N.H. fabricated the chips and N.H. performed the experiments; and M.A.D. and U.K. prepared the various buffered Locke's solution. N.H. and A.D.R. analyzed the data; E.S. performed the Bayesian analysis; N.H. and A.D.R. wrote the paper; and M.A.D. provided essential edits to the paper.

Notes

The authors declare no competing financial interest.

■ REFERENCES

(1) Bergveld, P. Development of an ion-sensitive solid-state device for neurophysiological measurements. *IEEE Trans. Biomed. Eng.* **1970**, *BME-17*, 70–71.

(2) Moser, N.; Lande, T. S.; Toumazou, C.; Georgiou, P. ISFETs in CMOS and emergent trends in instrumentation: A review. *IEEE Sens. J.* **2016**, *16*, 6496–6514.

(3) Martinoia, S.; Massobrio, G.; Lorenzelli, L. Modeling ISFET microsensor and ISFET-based microsystems: a review. *Sens. Actuators, B* **2005**, *105*, 14–27.

(4) Duroux, P.; Emde, C.; Bauerfeind, P.; Francis, C.; Grisel, A.; Thybaud, L.; Arstrong, D.; Depeursinge, C.; Blum, A. The ion sensitive field effect transistor (ISFET) pH electrode: a new sensor for long term ambulatory pH monitoring. *Gut* **1991**, *32*, 240–245.

(5) McLaughlin, K.; Dickson, A.; Weisberg, S. B.; Coale, K.; Elrod, V.; Hunter, C.; Johnson, K. S.; Kram, S.; Kudela, R.; Martz, T.; et al. An evaluation of ISFET sensors for coastal pH monitoring applications. *Reg. Stud. Mar. Sci.* **2017**, *12*, 11–18.

(6) Jimenez-Jorquera, C.; Orozco, J.; Baldi, A. ISFET based microsensors for environmental monitoring. *Sensors* **2010**, *10*, 61–83.

(7) Sandifer, J. R.; Voycheck, J. J. A review of biosensor and industrial applications of ph-isfets and an evaluation of honeywell's "durafet". *Microchim. Acta* **1999**, *131*, 91–98.

(8) Dvir, T.; Timko, B. P.; Kohane, D. S.; Langer, R. Nanotechnological strategies for engineering complex tissues. *Nat. Nanotechnol.* **2011**, *6*, 13.

(9) Toumazou, C.; Georgiou, P. Piet Bergveld-40 years of ISFET technology: From neuronal sensing to DNA sequencing. *Electron. Lett.* **2011**, *47*, S7–S12.

(10) Syu, Y.-C.; Hsu, W.-E.; Lin, C.-T. Field-Effect Transistor Biosensing: Devices and Clinical Applications. *ECS J. Solid State Sci. Technol.* **2018**, *7*, Q3196–Q3207.

(11) Chen, S.; Bomer, J. G.; Carlen, E. T.; van den Berg, A. Al2O3/silicon nanoISFET with near ideal Nernstian response. *Nano Lett.* **2011**, *11*, 2334–2341.

(12) Schöning, M. J.; Brinkmann, D.; Rolka, D.; Demuth, C.; Poghossian, A. CIP (cleaning-in-place) suitable "non-glass" pH sensor based on a Ta$_2$O$_5$-gate EIS structure. *Sens. Actuators, B* **2005**, *111–112*, 423–429.

(13) Bousse, L.; Mostarshed, S.; van der Schoot, B.; De Rooij, N. Comparison of the hysteresis of Ta2O5 and Si3N4 pH-sensing insulators. *Sens. Actuators, B* **1994**, *17*, 157–164.

(14) Cui, Y.; Wei, Q.; Park, H.; Lieber, C. M. Nanowire nanosensors for highly sensitive and selective detection of biological and chemical species. *Science* **2001**, *293*, 1289–1292.

(15) Stern, E.; Klemic, J. F.; Routenberg, D. A.; Wyrembak, P. N.; Turner-Evans, D. B.; Hamilton, A. D.; LaVan, D. A.; Fahmy, T. M.; Reed, M. A. Label-free immunodetection with CMOS-compatible semiconducting nanowires. *Nature* **2007**, *445*, 519.

(16) Allen, B. L.; Kichambare, P. D.; Star, A. Carbon nanotube field-effect-transistor-based biosensors. *Adv. Mater.* **2007**, *19*, 1439–1451.

(17) Sorgenfrei, S.; Chiu, C.-y.; Gonzalez, R. L., Jr; Yu, Y.-J.; Kim, P.; Nuckolls, C.; Shepard, K. L. Label-free single-molecule detection of DNA-hybridization kinetics with a carbon nanotube field-effect transistor. *Nat. Nanotechnol.* **2011**, *6*, 126.

(18) Knopfmacher, O.; Hammock, M. L.; Appleton, A. L.; Schwartz, G.; Mei, J.; Lei, T.; Pei, J.; Bao, Z. Highly stable organic polymer field-effect transistor sensor for selective detection in the marine environment. *Nat. Commun.* **2014**, *5*, No. 2954.

(19) Schmoltner, K.; Kofler, J.; Klug, A.; List-Kratochvil, E. J. Electrolyte-Gated Organic Field-Effect Transistor for Selective Reversible Ion Detection. *Adv. Mater.* **2013**, *25*, 6895–6899.

(20) Benfenati, V.; Toffanin, S.; Bonetti, S.; Turatti, G.; Pistone, A.; Chiappalone, M.; Sagnella, A.; Stefani, A.; Generali, G.; Ruani, G.; et al. A transparent organic transistor structure for bidirectional stimulation and recording of primary neurons. *Nat. Mater.* **2013**, *12*, 672.

(21) Ohno, Y.; Maehashi, K.; Yamashiro, Y.; Matsumoto, K. Electrolyte-gated graphene field-effect transistors for detecting pH and protein adsorption. *Nano Lett.* **2009**, *9*, 3318–3322.

(22) Dong, X.; Shi, Y.; Huang, W.; Chen, P.; Li, L. J. Electrical detection of DNA hybridization with single-base specificity using transistors based on CVD-grown graphene sheets. *Adv. Mater.* **2010**, *22*, 1649–1653.

(23) Spijkman, M. J.; Myny, K.; Smits, E. C.; Heremans, P.; Blom, P. W.; De Leeuw, D. M. Dual-gate thin-film transistors, integrated circuits and sensors. *Adv. Mater.* **2011**, *23*, 3231–3242.

(24) Go, J.; Nair, P. R.; Reddy, B., Jr; Dorvel, B.; Bashir, R.; Alam, M. A. Coupled heterogeneous nanowire−nanoplate planar transistor sensors for giant (> 10 V/pH) Nernst response. *ACS Nano* **2012**, *6*, 5972–5979.

(25) Bergveld, P.; DeRooij, N.; Zemel, J. Physical mechanisms for chemically sensitive semiconductor devices. *Nature* **1978**, *273*, 438.

(26) Van Hal, R.; Eijkel, J. C.; Bergveld, P. A novel description of ISFET sensitivity with the buffer capacity and double-layer capacitance as key parameters. *Sens. Actuators, B* **1995**, *24*, 201–205.

(27) Sivakumarasamy, R.; Hartkamp, R.; Siboulet, B.; Dufrêche, J.-F.; Nishiguchi, K.; Fujiwara, A.; Clément, N. Selective layer-free blood serum ionogram based on ion-specific interactions with a nano-transistor. *Nat. Mater.* **2018**, *17*, 464.

(28) Parizi, K. B.; Xu, X.; Pal, A.; Hu, X.; Wong, H. P. ISFET pH sensitivity: Counter-Ions play a key role. *Sci. Rep.* **2017**, *7*, No. 41305.

(29) Jamasb, S.; Collins, S.; Smith, R. L. A physical model for drift in pH ISFETs. *Sens. Actuators, B* **1998**, *49*, 146–155.

(30) Martz, T. R.; Connery, J. G.; Johnson, K. S. Testing the Honeywell Durafet for seawater pH applications. *Limnol. Oceanogr.: Methods* **2010**, *8*, 172–184.

(31) Merriman, B.; Torrent, I.; Rothberg, J. M. Progress in ion torrent semiconductor chip based sequencing. *Electrophoresis* **2012**, *33*, 3397–3417.

(32) Ang, P. K.; Chen, W.; Wee, A. T. S.; Loh, K. P. Solution-gated epitaxial graphene as pH sensor. *J. Am. Chem. Soc.* **2008**, *130*, 14392–14393.

(33) Hasan, N.; Hou, B.; Moore, A. L.; Radadia, A. D. Enhanced ionic sensitivity in solution-gated graphene-hexagonal boron nitride

heterostructure field-effect transistors. *Adv. Mater. Technol.* **2018**, *3*, No. 1800133.

(34) Yan, F.; Zhang, M.; Li, J. Solution-Gated Graphene Transistors for Chemical and Biological Sensors. *Adv. Healthcare Mater.* **2014**, *3*, 313−331.

(35) Loan, P. T. K.; Wu, D.; Ye, C.; Li, X.; Tra, V. T.; Wei, Q.; Fu, L.; Yu, A.; Li, L.-J.; Lin, C.-T. Hall effect biosensors with ultraclean graphene film for improved sensitivity of label-free DNA detection. *Biosens. Bioelectron.* **2018**, *99*, 85−91.

(36) Dean, C. R.; Young, A. F.; Meric, I.; Lee, C.; Wang, L.; Sorgenfrei, S.; Watanabe, K.; Taniguchi, T.; Kim, P.; Shepard, K. L.; et al. Boron nitride substrates for high-quality graphene electronics. *Nat. Nanotechnol.* **2010**, *5*, 722−726.

(37) Geim, A. K.; Grigorieva, I. V. Van der Waals heterostructures. *Nature* **2013**, *499*, 419.

(38) Kim, K.; Choi, J.-Y.; Kim, T.; Cho, S.-H.; Chung, H.-J. A role for graphene in silicon-based semiconductor devices. *Nature* **2011**, *479*, 338.

(39) Meric, I.; Dean, C. R.; Petrone, N.; Wang, L.; Hone, J.; Kim, P.; Shepard, K. L. Graphene field-effect transistors based on boron−nitride dielectrics. *Proc. IEEE* **2013**, *101*, 1609−1619.

(40) Moon, P.; Koshino, M. Electronic properties of graphene/hexagonal-boron-nitride moiré superlattice. *Phys. Rev. B* **2014**, *90*, No. 155406.

(41) Yankowitz, M.; Xue, J.; LeRoy, B. J. Graphene on hexagonal boron nitride. *J. Phys.: Condens. Matter* **2014**, *26*, No. 303201.

(42) Kovtyukhova, N. I.; Perea-López, N.; Terrones, M.; Mallouk, T. E. Atomically Thin Layers of Graphene and Hexagonal Boron Nitride Made by Solvent Exfoliation of Their Phosphoric Acid Intercalation Compounds. *ACS Nano* **2017**, *11*, 6746−6754.

(43) Pratik, K. C.; Rai, A.; Ashton, T. S.; Moore, A. L. APCVD hexagonal boron nitride thin films for passive near-junction thermal management of electronics. *Nanotechnology* **2017**, *28*, No. 505705.

(44) Choi, D. S.; Poudel, N.; Park, S.; Akinwande, D.; Cronin, S. B.; Watanabe, K.; Taniguchi, T.; Yao, Z.; Shi, L. Large Reduction of Hot Spot Temperature in Graphene Electronic Devices with Heat-Spreading Hexagonal Boron Nitride. *ACS Appl. Mater. Interfaces* **2018**, *10*, 11101−11107.

(45) Ghittorelli, M.; Lingstedt, L.; Romele, P.; Crăciun, N. I.; Kovács-Vajna, Z. M.; Blom, P. W.; Torricelli, F. High-sensitivity ion detection at low voltages with current-driven organic electrochemical transistors. *Nat. Commun.* **2018**, *9*, No. 1441.

(46) Masvidal-Codina, E.; Illa, X.; Dasilva, M.; Calia, A. B.; Dragojević, T.; Vidal-Rosas, E. E.; Prats-Alfonso, E.; Martínez-Aguilar, J.; Jose, M.; Garcia-Cortadella, R.; et al. High-resolution mapping of infraslow cortical brain activity enabled by graphene microtransistors. *Nat. Mater.* **2019**, *18*, 280−288.

(47) Morf, W. E. *The Principles of Ion-Selective Electrodes and of Membrane Transport.*; Elsevier, 2012; Vol. 2.

(48) Li, H.; Zhu, Y.; Islam, M. S.; Rahman, M. A.; Walsh, K. B.; Koley, G. Graphene field effect transistors for highly sensitive and selective detection of K+ ions. *Sens. Actuators, B* **2017**, *253*, 759−765.

(49) Maehashi, K.; Sofue, Y.; Okamoto, S.; Ohno, Y.; Inoue, K.; Matsumoto, K. Selective ion sensors based on ionophore-modified graphene field-effect transistors. *Sens. Actuators, B* **2013**, *187*, 45−49.

(50) Kim, J.; Wang, L.; Bourouina, T.; Cui, T. Ion sensitive field effect transistor based on graphene and ionophore hybrid membrane for phosphate detection. *Microsyst. Technol.* **2019**, *25*, 3357−3364.

(51) Li, P.; Liu, B.; Zhang, D.; Sun, Ye.; Liu, J. Graphene field-effect transistors with tunable sensitivity for high performance Hg (II) sensing. *Appl. Phys. Lett.* **2016**, *109*, No. 153101.

(52) Jin, C.; Kim, J.; Suh, J.; Shi, Z.; Chen, B.; Fan, X.; Kam, M.; Watanabe, K.; Taniguchi, T.; Tongay, S. Interlayer electron−phonon coupling in WSe₂/hBN heterostructures. *Nat. Phys.* **2017**, *13*, 127.

(53) Geick, R.; Perry, C.; Rupprecht, G. Normal modes in hexagonal boron nitride. *Phys. Rev.* **1966**, *146*, No. 543.

(54) Serrano, J.; Bosak, A.; Arenal, R.; Krisch, M.; Watanabe, K.; Taniguchi, T.; Kanda, H.; Rubio, A.; Wirtz, L. Vibrational properties of hexagonal boron nitride: inelastic X-ray scattering and ab initio calculations. *Phys. Rev. Lett.* **2007**, *98*, No. 095503.

(55) Casiraghi, C. Raman Spectroscopy of Graphene. In *Spectroscopic Properties of Inorganic and Organometallic Compounds: Techniques, Materials and Applications*; the Royal Society of Chemistry: London, U.K 2012; pp 29−56.

(56) Ferrari, A. C. Raman spectroscopy of graphene and graphite: disorder, electron−phonon coupling, doping and nonadiabatic effects. *Solid State Commun.* **2007**, *143*, 47−57.

(57) Malard, L.; Pimenta, M.; Dresselhaus, G.; Dresselhaus, M. Raman spectroscopy in graphene. *Phys. Rep.* **2009**, *473*, 51−87.

(58) Xia, J.; Chen, F.; Li, J.; Tao, N. Measurement of the quantum capacitance of graphene. *Nat. Nanotechnol.* **2009**, *4*, 505.

(59) Fang, T.; Konar, A.; Xing, H.; Jena, D. Carrier statistics and quantum capacitance of graphene sheets and ribbons. *Appl. Phys. Lett.* **2007**, *91*, No. 092109.

(60) Chen, F.; Qing, Q.; Xia, J.; Li, J.; Tao, N. Electrochemical gate-controlled charge transport in graphene in ionic liquid and aqueous solution. *J. Am. Chem. Soc.* **2009**, *131*, 9908−9909.

(61) Raimondo, J. V.; Burman, R. J.; Katz, A. A.; Akerman, C. J. Ion dynamics during seizures. *Front. Cell. Neurosci.* **2015**, *9*, No. 419.

(62) Schwartzkroin, P. A.; Baraban, S. C.; Hochman, D. W. Osmolarity, ionic flux, and changes in brain excitability. *Epilepsy Res.* **1998**, *32*, 275−285.

(63) Gao, W.; Emaminejad, S.; Nyein, H. Y. Y.; Challa, S.; Chen, K.; Peck, A.; Fahad, H. M.; Ota, H.; Shiraki, H.; Kiriya, D.; et al. Fully integrated wearable sensor arrays for multiplexed in situ perspiration analysis. *Nature* **2016**, *529*, 509.

(64) Bandodkar, A. J.; Molinnus, D.; Mirza, O.; Guinovart, T.; Windmiller, J. R.; Valdés-Ramírez, G.; Andrade, F. J.; Schöning, M. J.; Wang, J. Epidermal tattoo potentiometric sodium sensors with wireless signal transduction for continuous non-invasive sweat monitoring. *Biosens. Bioelectron.* **2014**, *54*, 603−609.